

Received June 30, 2021, accepted July 9, 2021, date of publication July 20, 2021, date of current version August 4, 2021.

Digital Object Identifier 10.1109/ACCESS.2021.3098974

Research on IGBT Bonding Wires Crack Propagation at the Macro and Micro Scales

JUN LUO¹, SHUKAI GUAN², BO WAN², (Member, IEEE), MAOGONG JIANG³,
AND GUICUI FU², (Member, IEEE)

¹Sichuan Institute of Solid-State Circuits, China Electronics Technology Group Corporation, Chongqing 400060, China

²School of Reliability and Systems Engineering, Beihang University, Beijing 100191, China

³China Aerospace Components Engineering Center, CASC, Beijing 100094, China

Corresponding author: Bo Wan (wanbo@buaa.edu.cn)

ABSTRACT Under the action of a complex and harsh working environment, the damage of the IGBT power module's packaging interconnection structure is the primary failure mode. The crack propagation and the bonding interface and the bond point shedding in the bonding wires will seriously affect the device's electrical interconnection function and heat dissipation ability, resulting in its performance degradation and failure. In this work, the formulation and application of a multiscale approach combined with a cohesive zone model (CZM) were proposed to investigate IGBT bonding wires' crack propagation. Firstly, the cohesive force model's principle considering fatigue damage accumulation is analyzed, and the degradation multiscale simulation method of the critical structure of the power module is studied. Secondly, further research on IGBT bonding wires' degradation behavior is carried out based on the macro and micro scales. The IGBT power module key package structure's defect evolution model is established to analyze the damage evolution process of the critical package structure. Finally, the accuracy of the model is verified by the experiment analysis. Such a multiscale, mechanism-based cohesive zone model offers a promising approach for modeling and understanding the rate-dependent fracture of IGBT bonding wire crack evolution.

INDEX TERMS IGBT power module, bonding wires crack degradation, cohesive zone model, multiscale model simulation.

I. INTRODUCTION

Power modules are critical in power electronic systems. The reliability of power devices [1] is of great concern in power electronics applications. Insulated Gate Bipolar Transistors (IGBTs) represent the third technological revolution of power semiconductor devices. It has the characteristics of large capacity, fast switching, high frequency and low loss. It is a critical device in many application fields such as weapon equipment, aerospace, rail transit and new energy. The essential base product strictly requires the life and reliability of IGBTs. In the actual long-term harsh working conditions, the silicon IGBT power module's most vulnerable position is the connection part of the package structure. It mainly includes the module welding layer structure and the bonding point between the bonding wires and the chip surface. The degradation failure of these positions is the main factor affecting the reliability of power devices.

The associate editor coordinating the review of this manuscript and approving it for publication was Cristian Zambelli¹.

In terms of reliability evaluation of IGBT power devices, a large number of researches use life models to estimate the service life of devices under the task profile, such as Coffin Manson model [2], Paris model [3] and other life prediction models to estimate the structural life of devices. On this basis, the lifetime of power devices can also be modified in the Coffin Manson model to consider the influence of factors such as power cycle frequency, maximum junction temperature, bonding wire diameter, load current, heating time, etc., such as the Norris-Landzberg model [4] and Bayerer model [5]. Y. Celnikier et al used FEM and some analytical developments, the IGBT bonding wires heel crack mechanism appearing in service, and established that the initial residual stresses contribute to limit the wire/ribbon lifetime [6]. Another widely used method is the time-domain reliability physical model considering the cumulative effect of fatigue. Based on this theory, Yang *et al.* considered the plastic behavior of bonded leads and established the damage function to obtain the relationship between the crack length and the cyclic load [7]. Lai W *et al.* also used this theory to analyze the crack

length in the welding layer structure of the IGBT module chip and established the module life prediction method under the condition of a long time, narrow temperature and power cycle [8]. These methods have established prediction models for device life in different temperature ranges, but they also have some limitations. Most of the life prediction model parameters are determined based on a large amount of life or performance degradation test data. Due to the limited test support data for different packaging types or geometric sizes, it is difficult to determine some formula coefficients. In addition, the life prediction model cannot describe the whole process of crack initiation, propagation and final failure in the package structure. At present, relatively few scholars have studied this aspect.

The reliability analysis and evaluation of IGBT power module packaging structure is a problem involving multiple physical fields. The power loss generated by the current generates a lot of heat in the device, which causes the internal structural stress of the device to be uneven until it is completely damaged and fails. Therefore, to accurately obtain the displacement information of the module structure under cyclic loading, it is necessary to establish a macro-scale multi-physics coupling model.

In order to analyze the damage degradation process and life expectancy of the critical package structure in the IGBT power module, the overall model is usually used for numerical simulation analysis of the macroscopic temperature or stress-strain distribution. The established IGBT life model can also be used to predict life. These methods ignore the underlying physical mechanism of crack initiation and propagation. The bond wires in the IGBT power module are made of metal materials for electrical and heat transfer functions. At present, existing methods include The Virtual Crack Closure Technique (VCCT); The Cohesive Zone Model (CZM); and The Extended Finite Element Method (XFEM). The VCCT is relatively mature, but it has several disadvantages: The mesh is very dense near the tip of the interface crack. A crack of known shape and size needs to be prefabricated in the structure; Complex mobile grid technology is required [9]. The CZM can simulate the whole process of crack initiation and propagation without presetting the initial crack under complex load and boundary conditions [10]. The XFEM can solve most of the simulation problems of structural, mechanical behavior. Still, it has certain limitations for large local stress and strain field gradient or the occurrence of multiple cracks and cracks propagation [11].

In this paper, the degradation behavior of the bonding wires of IGBT power modules is studied based on multi-scale simulation. On the macroscale, an electro-thermo-mechanical FEM-based model for IGBT modules is established in ABAQUS. The aim is to identify the degenerative process of bonding wires in IGBT power modules through simulations. On the microscale, the CZM is used to analyze the degradation behavior of the bonding wires. Based on the macro node displacement information, after the sensitive damage location is identified, thin cracks are successively inserted at the

interface to simulate the crack propagation. The law of crack initiation and growth length of power module bonding wires based on microstructure degradation is obtained. The defect evolution model of the bonding wires of the IGBT power modules is established by multi-scale simulation analysis. Finally, the correctness of the simulation results is verified through experiment analysis.

The remaining part of the paper proceeds as follows. Section 2 proposed a multiscale IGBT finite element simulation analysis method. In Section 3, the macro-scale modeling and simulation were performed, and the results were analyzed. In Section 4, the CZM was used to analyze the degradation behavior of the bonding wires. An experimental validation was presented to verify the effectiveness of this approach in Section 5. Conclusions were summarized in Section 6.

II. MULTISCALE IGBT FINITE ELEMENT SIMULATION ANALYSIS METHOD

A. STRUCTURAL MATERIAL AND PROCESS ANALYSIS

IGBT power module realizes electrical interconnection between a power semiconductor chip and external port through bonding wires. The diameter range of thick bonding wires is generally $300\ \mu\text{m} \sim 400\ \mu\text{m}$. In the power module, it is mainly used to connect the gate and its corresponding external pin.

In the chip emitter and its external pin and collector path in the power module, rough bonding wires are used to realize the connection between copper and the outer electrode. Due to its good conductivity, corrosion resistance and low price, high purity aluminum bonding wires have become one of the leading application technologies of current power device packaging. In power modules, multiple coarse aluminum bonding wires are usually used side by side to meet current transmission requirements. Typical coarse aluminum bonding wires of power modules are shown in FIGURE 1.

For ease of interpretation of this and subsequent virtual cross sections, it may be helpful to refer to the schematic representation in FIGURE 2.

FIGURE 3 shows the damage of the IGBT power module's internal structure after the power cycle test. It can be observed that multiple bonding wires fall off obviously. In contrast, the bonding force of the bonding wires without significant fall-off is significantly lower than that of the new module bonding wires.

B. IGBT BONDING WIRES DEGRADATION SIMULATION METHOD

To analyze the relationship between crack propagation behavior and cyclic load in the IGBT power module package structure and the typical application conditions of the power module from a microscopic perspective, a set of degradation simulation methods for the vital package structure of multi-scale IGBT power modules have been established. The overall analysis flow is shown in FIGURE 4. It mainly includes

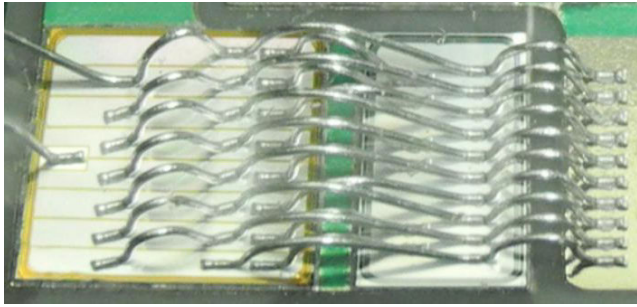


FIGURE 1. Typical power module aluminum bonding wires.

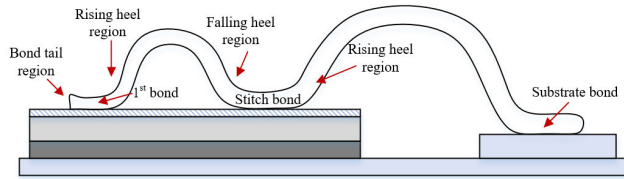


FIGURE 2. Region definition of bonding wires.

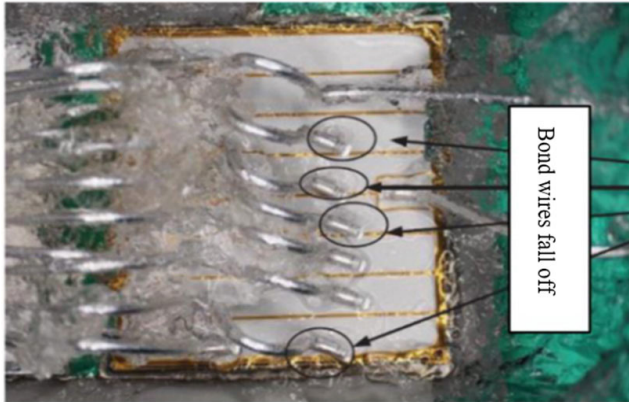


FIGURE 3. IGBT power module bonding wires fall off.

three parts: the analysis of IGBT power module packaging structure material and process information, the simulation of macro-scale structure deformation and the simulation of micro-scale crystal crack growth.

First, we analyze the key package structure size information of the IGBT power module, including the laminated structure, bonding wire structure and internal crystal structure information. Investigate and analyze the material properties at the macro and micro levels, and analyze the influence of the manufacturing process of the device on the internal material properties of the device.

At the macro scale, IGBT power module works under the condition of repeated turn-on and turn-off electrical stress, the chip generates heat, which leads to the stress change of the internal structure of the device, and then forms the structure damage and evolution. The finite element analysis model under the condition of multi-physics coupling is established in the ABAQUS software. Determine the location most likely to cause structural damage by analyzing information such as stress and strain, and obtain displacement information of key nodes.

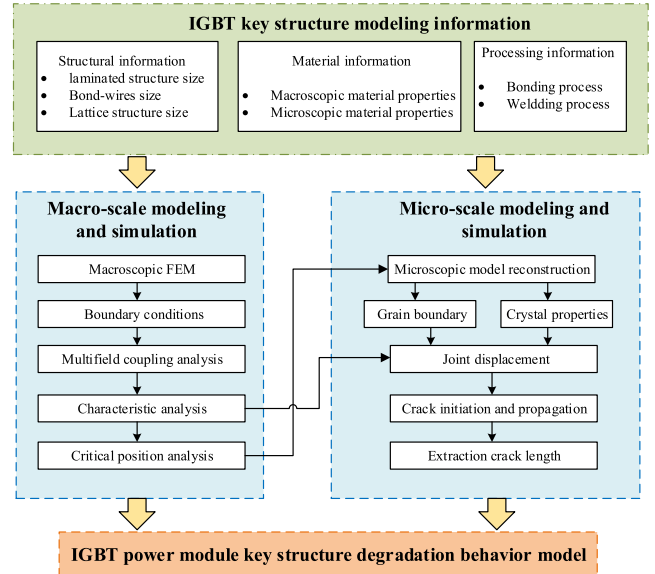


FIGURE 4. Process of multiscale finite element simulation analysis for key package structure of IGBT.

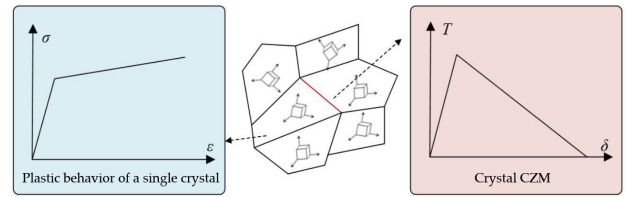


FIGURE 5. Models used in crystal structure simulation for internal and inter crystal boundaries.

Under the actual working conditions, the actual structure degradation process of materials is very complex. The fracture modes may include intergranular fracture and transcrystalline fracture. To obtain the crack propagation law in the key packaging structure of IGBT power devices, the following assumptions are made in the finite element analysis [12]. 1) There are no defects in the crystal. 2) Only intergranular fracture is considered in the fracture mode.

In terms of microscale, the node displacement information of the macro-scale model is used as the boundary condition of the micro model to reconstruct the micro-model. To comprehensively describe the behavior of microscopic materials, the characteristics of crystal interior and crystal boundary need to be considered, as shown in FIGURE 5. The CZM is adopted between crystals, and anisotropic plastic strain should be considered within grains.

There are mainly two ways to describe the plasticity of crystals and their anisotropy [13], [14]. Because the anisotropic yield function method is more efficient, we use the yield function method to simulate the crack propagation process of IGBT key encapsulated structure.

The grains' characteristics in the structure are random, and the grains generate random patterns according to the Voronoi diagram. The crystal size distribution of metals $f(d)$ is characterized by the lognormal distribution probability density

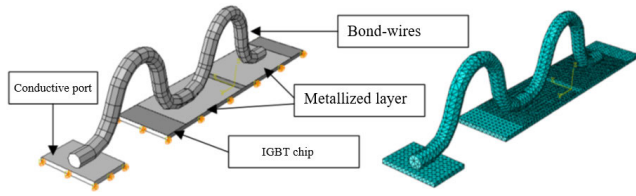


FIGURE 6. Finite element model structure and meshing results of bonding wires.

function in the form of the formula (1).

$$f(d) = \frac{1}{\sigma\sqrt{2\pi}d} \exp\left[\frac{-(\ln d - \mu)^2}{2\sigma^2}\right], \quad d > 0 \quad (1)$$

where d is the crystal size, μ is the mean value, and σ is the standard deviation. These parameters can be used to perform statistical analysis of the crystal characteristics of the area of interest through techniques such as EBSD to obtain the crystal size and crystal orientation distribution characteristics, which can be used as input information for generating the microscale structure.

III. MACROSCALE MODELING AND SIMULATION

A. SIMULATION ANALYSIS

1) MODELING

The IGBT power module uses multiple bonding wires in a parallel arrangement. To facilitate the study of the internal degradation of the bonding wires, a single bonding wire structure is extracted from the typical IGBT power module geometry structure as the research object of this part.

To reduce the computation time, the geometric structure of the model is simplified. The geometric structure of bonding wire and mesh generation results are shown in FIGURE 6. The model mainly consists of bonding wires, metallization layer, IGBT chip and conductive port.

In the overall model of bonding wires structure, the metallized layer and the conductive port are aluminum metal IGBT chip and silicon. All the material parameters used are shown in Table 1 [15], [16]. For high-purity aluminum bonding wire, when the temperature fluctuation range exceeds 10K, plasticity should be considered to study its degradation process [17], so aluminum material is set as a plastic material property.

The temperature-dependent parameters σ_{Si} and k_{Si} of the material are given, respectively, as., the electrical conductivity σ_{Si} can be fitted as

$$\sigma_{Si} = 4.15 \times 10^5 \times T^{-1.41} [S/m] \quad (2)$$

$$k_{Si} = 2.52 \times 10^5 \times T^{-1.3} [W/(m \cdot K)] \quad (3)$$

where T is the temperature in Kelvin.

2) SIMULATION AND RESULTS

In the macro analysis model of the IGBT power module bonding wire, electrical, thermal and structural fields are mainly considered. In the analysis step of ABAQUS, the physical coupling field of heat-electric-structure was selected, and the grid cell type was set as Q3D4. In terms of boundary

TABLE 1. Material parameters used in the integral model of bonding wires structures.

Property	Symbol	Unit	Si	Al
Density	ρ	kg/m ³	2330	2690
Conductivity	σ	S/m	Eq.(2)	3.7e7
Heat conductivity	k	W/(m·K)	Eq.(3)	238
Specific heat	Cp	J/(kg·K)	700	900
Young modulus	E	GPa	162.7	68
Poisson ratio	τ	1	0.28	0.30
Yield strength	σ_{yield}	MPa	-	30
Tangent modulus	τ_{tan}	MPa	-	216

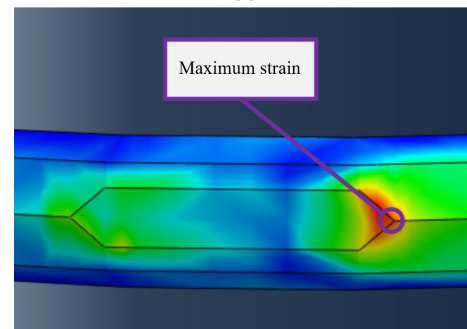
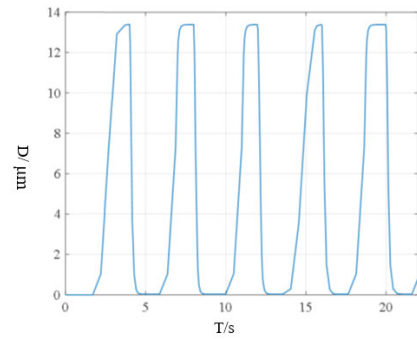


FIGURE 7. Macro scale simulation results: (a) Maximum displacement curve (the highest point of the bonding wire); (b) Cloud map of plastic strain distribution at the interface between the bonding wire and chip.

conditions, the electrical side applies periodic input current under the silicon chip, and the bottom of the other electrical port is set as ground. In terms of thermal boundary, heat dissipation conditions are set at the bottom of the overall structure, and the surface is for air convection heat dissipation. At the bottom of the whole model, the structural field is fixed in X , Y and Z directions.

Taking the load and boundary conditions of input currently 55A, current applied time 2s, device turn-off time 2s, and ambient temperature 293.15K as examples, the simulation results obtained by specific analysis are shown in FIGURE 7. The maximum displacement point of the bonding wire is the highest arc point of the bonding wire. The displacement of the extracted point is shown in FIGURE 7(a). The maximum displacement is 13.118 μ m; Under the repeated action of periodic current load, the maximum plastic strain position on the bonding lead is at the interface between the bottom of the wedge structure and the chip surface and is located at the edge of the bonding position. The strain

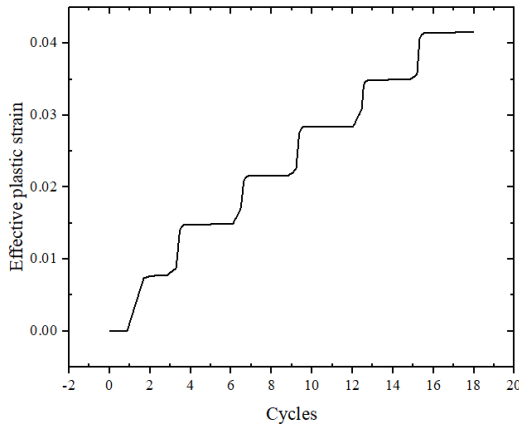


FIGURE 8. Relationship between effective plastic strain accumulation and number of cycles.

TABLE 2. Main parameters of the IGBT power module used in the case application.

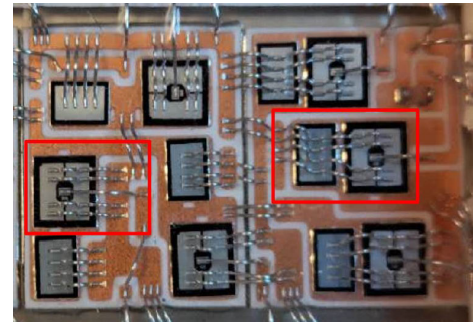
Parameter Name	Symbol	Test Conditions	Numerical Value
Collector emitter voltage	V_{CES}	$T_j = 25^\circ\text{C}$	1200V
Continuous collector DC current	I_{Cnom}	$T_c = 95^\circ\text{C}, T_{jmax} = 175^\circ\text{C}$ $I_c = 50\text{A}, V_{GE} = 15\text{V}, T_j = 25^\circ\text{C}$	50A 1.85V
Collector-emitter saturation voltage	V_{CEsat}	$I_c = 50\text{A}, V_{GE} = 15\text{V}, T_j = 125^\circ\text{C}$ $I_c = 50\text{A}, V_{GE} = 15\text{V}, T_j = 150^\circ\text{C}$	2.15V 2.25V
Gate threshold voltage	V_{Gth}	$I_c = 1.70\text{mA}, V_{CE} = V_{GE}, T_j = 25^\circ\text{C}$	5.8V

distribution at the bottom of the bonding wire is shown in FIGURE 7(b).

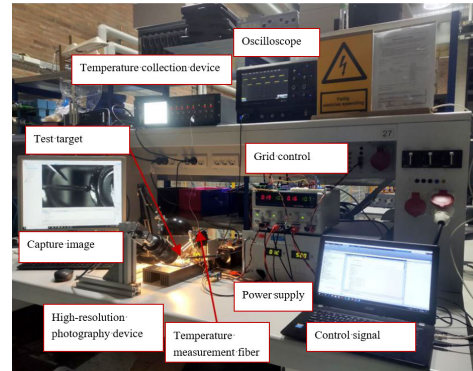
Extract the relationship between the effective plastic strain at the maximum strain and the number of cycles, as shown in FIGURE 8. The effective plastic strain inside the bonding wire accumulates with the increase of the number of load cycles. The maximum effective plastic strain increment at the edge of the bonding interface tends to a stable value after two cycle profiles.

B. VERIFICATION OF MACRO SIMULATION RESULTS

In this paper, a certain 1200 V and 50 A three-phase IGBT power integration module is selected as a specific object to carry out experiment application research. The module includes six groups of IGBT chips and reverses free-wheeling diodes and other auxiliary circuits. The package interconnection structure of the IGBT power module is a typical multi-bonding wire and multi-bonding point. The main parameters are shown in Table 2. This power module is widely used in fields such as motor control and drive, etc., and the same bonding wire is adopted as described in the analysis. Some IGBT chips are selected to carry out experiment application and research, as shown in FIGURE 9(a). Based on the IGBT power module test circuit, using optical fiber temperature sensors and high-precision photography equipment,



(a)



(b)

FIGURE 9. Test components and equipment: (a) The IGBT power module in the test; (b) Bonding wire temperature and structural deformation measurement test.

a lead temperature test and deformation test device, as shown in FIGURE 9(b), was built. Use an optical fiber thermometer to measure the highest point’s temperature on the bonding wire to verify the model.

Use a high-resolution camera (acA3800-14 μm) to observe the IGBT power module bonding wire’s mechanical deformation under working conditions. The image of the bonding wire structure can be obtained and post-processed in the Labview program. It is measured that the diameter of the bonding wire of the tested IGBT power module is 400 μm , and the transparent silica gel in the module is chemically removed to eliminate the influence of light refraction of the silica gel during heating and cooling. The maximum lead displacement d_{move} in the image can be obtained as

$$d_{move} = \phi_{wire} \frac{L_{move}}{L_{wire_dia}} \tag{4}$$

ϕ_{wire} is the diameter of the bonding wire, L_{move} is the pixel value of the wire deformation in the image, and L_{wire_dia} is the pixel value of the wire diameter in the image.

Assuming that the angle between the camera and the vertical support arm is α , the actual maximum displacement value of the bonding wire d_{real} can be expressed as:

$$d_{real} = \frac{d_{move}}{\sin \alpha} \tag{5}$$

In the test, the module’s overall image and the image at the maximum arc height of the bonding wire were captured, as shown in FIGURE 10. This result is useful to improve

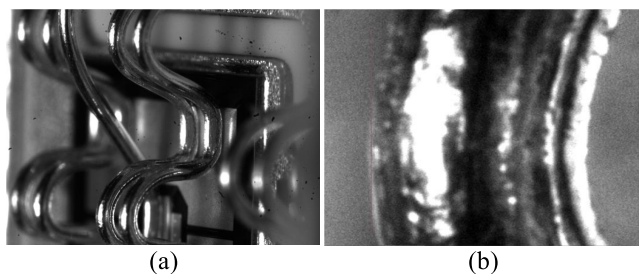


FIGURE 10. Images taken by high-speed photography equipment: (a). Bonding wires deformation measuring test device; (b). Top detail image of the bonding wires.

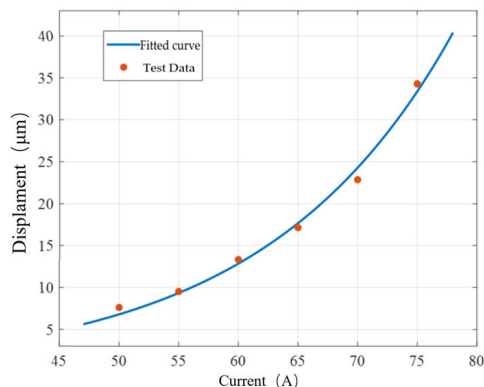


FIGURE 11. The relationship between the deformation displacement of the highest point of the bonding wire and the magnitude of the load current.

the predictive capabilities in mono-scale modeling of bonding wires failure, due to crack propagation. Thus, in phenomenological models based on the cohesive crack method both constitutive relations, the continuum stress-strain model and the discrete cohesive law, should be adapted through the incorporation of an estimated measure of the tortuosity in the smaller length scales.

In the experiment, the angle α between the high-resolution photography equipment and the vertical support is 50° . The loaded load current is within the range of 50 A~75 A, and the maximum displacement of the bonding wire is measured at every interval of 5 A. The data obtained are shown in Table 3. The relationship between the deformation displacement at the highest point of the bonding wire and the magnitude of the load current is shown in FIGURE 11.

The relationship between the maximum displacement of the bonding wire and the load current obtained by fitting is as follows.

$$d = 0.2824 \times \exp(0.06363 \times I_c) \quad (6)$$

The goodness of fit between the calculated fitted value and the actual measured value is 0.9917. This relationship can describe the relationship between the maximum displacement of the highest point of the bonding wire and the total load current. The established macroscale finite element analysis model has been calibrated and verified through the test data.

TABLE 3. The highest point displacement of the lead under different load currents.

Load current value	50A	55A	60A	65A	70A	75A
Displacement on the image	5.836	7.295	10.211	13.133	17.512	26.263
Actual maximum displacement	7.618	9.520	13.335	17.142	22.860	34.281

IV. MICROSCALE MODELING AND SIMULATION

A. CONSTITUTIVE RELATION OF CZM

In practice, many small cracks are generated due to the stress concentration at the crack front during the fracture process. The small crack enlarges with the stress until the small crack near the crack tip is connected with the main crack. The process in which the crack tip is constantly connected with the main crack is characterized by crack propagation. The process of crack formation and propagation can be simplified as the Cohesive Zone Model. This model is mainly based on the model proposed by Dugdale [18] and Barenblatt [19], [20] in the 1860s when they studied atomic lattice cohesion and simulated the deformation and fracture process of materials near the crack tip. CZM is considered to be one of the most effective methods to simulate and predict the structural degradation process [21]. At present, existing applications include two-dimensional simulation of the overall structure of the degraded solder layer of power devices [22], crystal level simulation of the substrate solder layer [23], integrated circuit interconnect structure integrity analysis [24], and cracks in the post-process laminar structure [25], etc. It is usually used to study the degradation behaviors such as delamination, fracture and debonding under static, dynamic and periodic loads [26].

In the research on the degradation of the IGBT power module’s essential package structure, the CZM can be used to analyze the crack growth process and then predict fatigue life. Compared with the traditional life prediction theory, the CZM can better describe the key package structure’s damage evolution process and reveal the crack law from the under-lying mechanism.

1) TENSION-DISPLACEMENT RELATION OF CZM

The main idea of the CZM is to assume that it is in front of the crack tip. A skinny interfacial layer with unique material properties exists between two adjacent entities. When a characteristic quantity used on the coating reaches the threshold, it will damage the layer structure until the layer structure completely fails. The structural unit is judged to disappear. The failure mode is manifested as a structural fracture in the overall model. Damage evolution occurs by in-creasing external stress or periodic loading. The model can describe the whole process of crack initiation and propagation.

The essence of cohesion is the interaction between atoms and molecules of matter. The typical crack tip growth process is shown in FIGURE 12. The CZM can include the front part of the crack tip (Forward), which is the region between A and

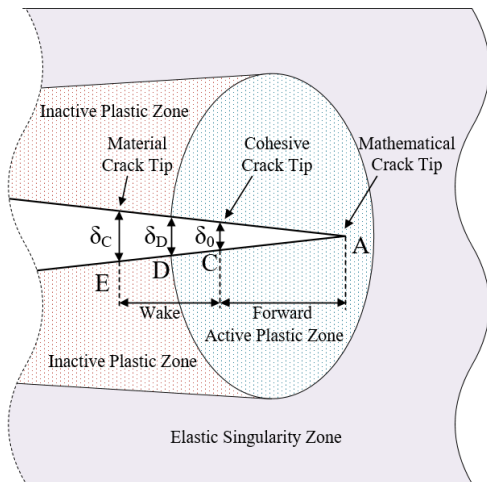


FIGURE 12. Property of material near crack.

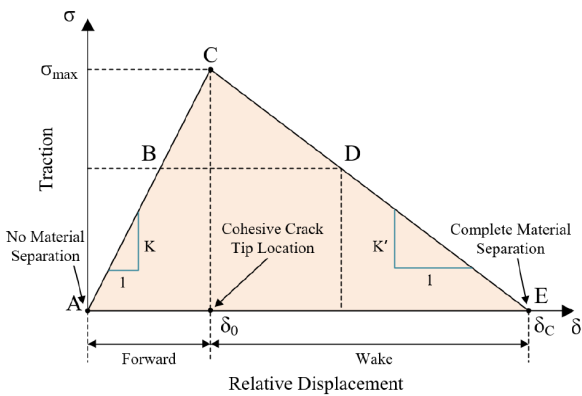


FIGURE 13. The tension-displacement relationship of the bilinear CZM.

C in the figure, and the weakening region (Wake), which is the region between C and E in the figure, which is the process of inhibiting crack growth.

The core of the CZM is to describe the damage or fracture process of the structure with the stress-displacement relationship in the local area [27]. This relation can be described in many ways, including bilinear, exponential, trapezoid and polynomial. In order to reduce the calculation cost, this paper adopts the bilinear CZM. The tension-displacement relationship of the bilinear CZM is shown in FIGURE 13, Correspond to the critical locations marked in FIGURE 12. Point A is the position where separation has not occurred. During the cohesive region's initial loading, the coherent force increases with the increase of the displacements at the cracked interface. Point C is the maximum tension position. After passing point C, the cohesion decreases gradually with tension displacement, until the position corresponding to point E is zero, and complete separation occurs.

The slope K of the AC segment is the linear segment stiffness of the model. The area bounded between the tension-displacement curve, and the abscissa is the cohesion energy. It represents the critical energy release rate of energy dissipation during crack opening G_C . The formula (7) of the bilinear

model can be expressed as

$$G_C = \int_0^{\delta_C} \sigma d\delta = \frac{1}{2} \sigma_{\max} \cdot \delta_C \quad (7)$$

In the formula: σ for tension, δ for displacement, σ_{\max} for material strength, δ_C for the displacement at complete separation.

In the bilinear model, the relation between tension and displacement during the hardening and softening of materials can be expressed as the formula (8).

$$\sigma = \begin{cases} \sigma_{\max} \frac{\delta_C}{\delta_0}, & \delta \leq \delta_0 \\ \sigma_{\max} \frac{\delta_C - \delta}{\delta_0 - \delta_0}, & \delta > \delta_0 \end{cases} \quad (8)$$

In the formula: δ_0 is the displacement of the cohesive force unit corresponding to the maximum tension.

For tangential and normal, the mixed-mode needs to be considered, as shown in FIGURE 14. The calculation between tension and displacement of cohesive force element is shown in Formula (9).

$$\begin{Bmatrix} \sigma_n \\ \sigma_s \\ \sigma_t \end{Bmatrix} = \begin{bmatrix} K_{nn} & 0 & 0 \\ 0 & K_{ss} & 0 \\ 0 & 0 & K_{tt} \end{bmatrix} \begin{Bmatrix} \sigma_n \\ \sigma_s \\ \sigma_t \end{Bmatrix} \quad (9)$$

In the formula: $\sigma_n, \sigma_s, \sigma_t$ are the stress values of cohesion units in normal and tangential directions, respectively. K_{nn}, K_{ss}, K_{tt} are the cohesion element stiffness of normal and tangential direction, the slope at the elastic stage of the middle line in FIGURE 13. $\sigma_n, \sigma_s, \sigma_t$ are the displacements of the cohesion units in the normal and tangential directions.

$$\left(\frac{\langle t_n \rangle}{t_n^0} \right)^2 + \left(\frac{\langle t_s \rangle}{t_s^0} \right)^2 + \left(\frac{\langle t_t \rangle}{t_t^0} \right)^2 = 1 \quad (10)$$

$\langle \rangle$ is MacAulay bracket, Their logic concerns $\langle t_n \rangle = 1/2 \cdot (t_n + |t_n|)$. For linear softening, damage evolution variable D proposed by Camanho and Davila is used to define degradation.

$$D = \frac{\delta_m^f (\delta_m^{\max} - \delta_m^0)}{\delta_m^{\max} (\delta_m^f - \delta_m^0)} \quad (11)$$

δ_m^{\max} is to reach the maximum relative displacement interface. In the initial state, the initial value of damage variable D is 0. After the damage starts, D increases gradually with the load's application until the maximum value is 1. When $D = 1$, the cohesion unit completely fails and the interface cracks and loses its carrying capacity. At this time, the element's stiffness is completely deleted from the overall stiffness matrix in ABAQUS, resulting in the fracture.

2) CUMULATIVE DAMAGE CRITERIA FOR CZM

Under the repeated action of cyclic load, the cohesive force unit will follow the tension - displacement relationship with degradation characteristic as the number of cycles increases.

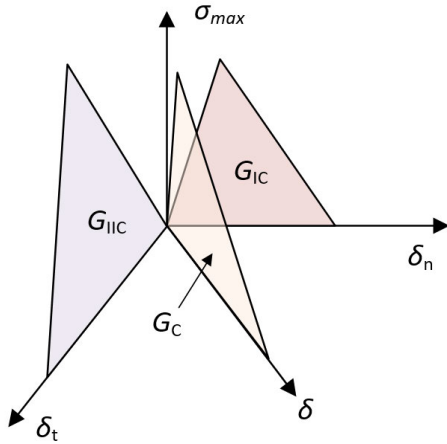


FIGURE 14. Bilinear tension - displacement relationship in mixed mode.

According to the damage theory proposed by Roe and Siegmund [27], the cohesion model considering damage degradation under cyclic loading can be expressed as

$$\begin{aligned} \sigma_{n,max} &= \sigma_{n,max m,0}(1 - D) \\ \sigma_{s,max} &= \sigma_{s,max m,0}(1 - D) \end{aligned} \quad (12)$$

In the formula: σ_n, σ_s are the initial maximum normal tension and the initial maximum tangential tension. D is the damage factor. In order to calculate the current damage state, a damage variable $\dot{D} = \dot{D}(T, \Delta u, D)$ is introduced to describe the damage process. Damage factors can be divided into two parts: fatigue damage variable \dot{D}_c under cyclic loading and damage variable \dot{D}_m under monotone loading [28].

$$\dot{D}_c = \frac{|\Delta \dot{u}|}{\delta_\Sigma} \left[\frac{\bar{\sigma}}{\sigma_{max}} - C_f \right] H(\Delta \bar{u} - \delta_0) \quad (13)$$

The damage variable is a value greater than or equal to 0. $\Delta \bar{u}$ is the change in displacement.

δ_Σ for damage threshold, is the scaling factor to calculate the damage caused by the increment of effective displacement. σ_{max} is the maximum tension in the current model. It corresponds to point C in FIGURE 14. C_f is the number between [0, 1], which represents the ratio between the stress amplitude of damage and the initial maximum stress that can be calculated. H is the Heaviside step function. $\Delta \bar{u}$ is the resultant displacement. δ_0 is cohesion model, the characteristics of the displacement and corresponding FIGURE 14 C point.

$$\begin{aligned} \Delta \bar{u} &= \sqrt{\Delta u_n^2 + \Delta u_t^2} \\ \Delta \dot{u} &= \Delta \bar{u}_t - \Delta \bar{u}_{t-\Delta t} \end{aligned} \quad (14)$$

Synthesis of $\bar{\sigma}$ tension can be expressed as

$$\bar{T} = \sqrt{T_n^2 + T_t^2 / (2eq^2)} \quad (15)$$

where $2eq^2$ is the proportional weight of tension in different directions.

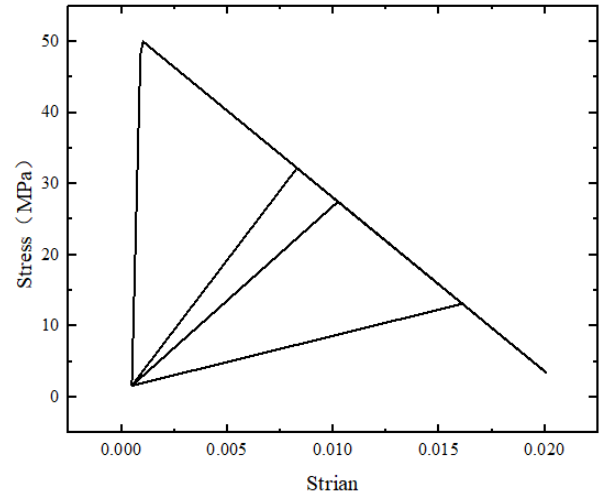


FIGURE 15. Stress-strain relationship obtained by cohesion model considering damage accumulation.

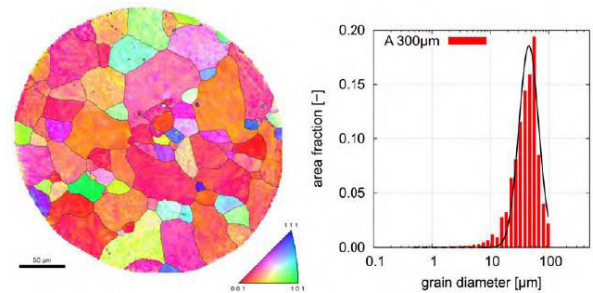


FIGURE 16. Typical crystal structure and size distribution of bonding wires.

When the maximum displacement increment $\Delta \bar{u}_{t-\Delta t}$ between the current displacement and the previous displacement is greater than the characteristic displacement δ_0 , the damage increment MD under monotone load can be expressed as

$$\dot{D}_M = \frac{\max(\Delta \bar{u}) - \max(\Delta \bar{u}_{t-\Delta t})}{4\delta_0}, \quad \text{if } \max(\Delta \bar{u}_{t-\Delta t}) > \delta_0 \quad (16)$$

The overall damage value D is the integral value of the maximum damage value of fatigue load and monotone load as follows.

$$D = \int \max(\dot{D}_c, \dot{D}_M) dt \quad (17)$$

The above cohesion model for describing material damage under cyclic loading uses ABAQUS user subroutine UMAT to embed material properties. The fundamental stress-strain relationship is shown in FIGURE 15.

B. SIMULATION ANALYSIS

According to the macro-scale simulation analysis results, the wedge-shaped part of the IGBT power module bonding wire and the semiconductor chip is the concentrated plastic strain. Therefore, the bonding wire model's wedge-shaped

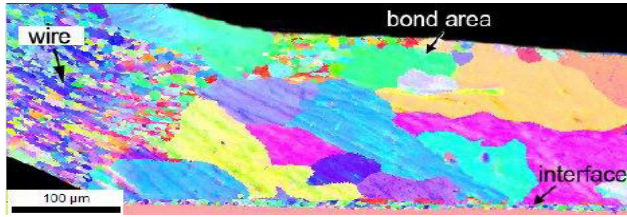


FIGURE 17. Microstructure after bonding process.

structure can be replaced by the micro-scale crystal model for further analysis. The interior of the aluminum bonding wire consists of a large number of aluminum metal grains. Electron Backscattering Detection (EBSD) of the lead’s typical grain structure is shown in FIGURE 16. On the right is the crystal size distribution, and the ratio of average crystal size to lead diameter is about 0.15 [29].

The wedge structure is divided into two parts to describe the crystal characteristics of the bonding site: the upper part of the wedge is mainly composed of 100~200 μm grain size, At the positions close to the metallized layer on the chip surface (about 10% of the overall height) and the upper regions away from the bonding point, the grain size was smaller, and the grain direction was different, as shown in FIGURE 17 [30]. It could be seen that the initial bonding wire was significantly separate from the crystals in the wedge structure.

The cohesion model has been applied to the bonding wire structure’s degradation simulation analysis from a macro perspective [31]. By inserting the cohesion model at the bonding interface and introducing the damage accumulation model, the relationship between the crack growth at the bonding interface and the cyclic temperature load was obtained.

The bonding structure is analyzed first, and the spatial position of the wedge structure in the bonding wire is calculated. Use the domain morphology method to generate the envelope plane in Neper.

$$d_i = a_i x + b_i y + c_i z \tag{18}$$

(a_i, b_i, c_i) is required to be a normal vector pointing to the outside of the domain space; The form of the plane coefficient information is (d_i, a_i, b_i, c_i) , where i is the number of the envelope plane. In order to analyze the micro-degradation law of the wedge-shaped structure of the bonding wire, we used 19 planes to form the envelope space. In this range, a microscopic model is established for simulation analysis of inter-grain crack growth.

Write a Matlab program for generating three-dimensional non-uniform crystal seed points. According to the grain size distribution characteristics in the wedge-shaped structure, random seed points for generating the crystal structure are generated in the envelope surface, as shown in FIGURE 18.

Then, it was imported into the Neper software and the Phon plug-in to generate random grains, insert the cohesion model, divide the grid, and create the simulation model structure, as shown in FIGURE 19. FIGURE 19(a) shows the aluminum

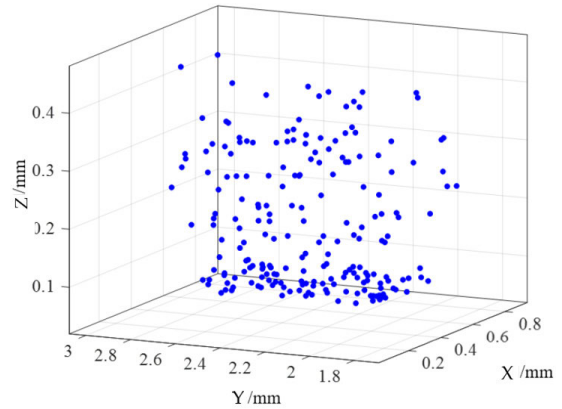


FIGURE 18. Envelope surface and seed point generated in Matlab.

TABLE 4. Anisotropic material properties of aluminum grains.

Young's modulus	$E_1 = 72GPa$	$E_2 = 42GPa$	$E_3 = 42GPa$
Shear modulus	$G_{12} = 26.9GPa$	$G_{13} = 20.0GPa$	$G_{23} = 20.0GPa$
Poisson's ratio	$\mu_{12} = 0.33$	$\mu_{13} = 0.25$	$\mu_{23} = 0.25$
Crystal orientation range	[0, π] the random number range		

grain structure; FIGURE 19(b) offers the boundary layer between the crystal grains, a cohesive unit with a thick-ness of zero.

Using the ABAQUS software, set the grain direction parallel to the grains’ bonding order near the bonding interface. The crystal grains on the upper side away from the bonding interface are given random crystal orientation according to the original bonding wire material’s characteristics.

By investigating the related literature on the mechanical properties of polycrystalline aluminum materials and bonding wire crystal materials, the anisotropic material properties of high-purity aluminum crystals can be obtained as shown in Table 4 [32].

Due to the uneven grain size after bonding, the size effect described by the Hall-Petch relationship should be considered, which satisfies the following form [33]:

$$\sigma_Y = \sigma_0 + \frac{k}{\sqrt{d}} \tag{19}$$

σ_Y is the yield stress when the material is deformed by 0.2%; σ_0 is the lattice friction resistance when a single dislocation is moved along the slip plane; k is a constant; d is the grain diameter, that is, the larger the grain size, the smaller the yield stress. The σ_0 in the Hall-Patch model is 16.8, and the k value is 3.5 [34]. In the area where cracks may appear (parallel and close to the bonding interface) [35]. Insert the cohesion unit of the unit properties shown in Table 5 between the aluminum crystal structures to realize the simulation of crack propagation.

Crack growth behavior [36] can be seen in the section diagram of bonding wires after ageing is shown in FIGURE 20. Crystal distribution and crack growth also have the following

TABLE 5. Cohesion unit properties between aluminum crystals.

Parameter name	Symbol	Value
Damage initial stress	t_p	500MPa
Energy release rate	G_C	0.15N/mm
Cohesion unit stiffness	k_a	10^5 MPa

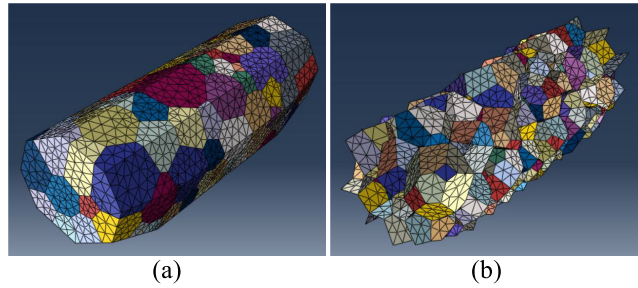


FIGURE 19. Neper generates the wedge structure model of bonding wires: (a) grain structure; (b) Grain boundary cohesion unit.

laws: a. In the metallized portion, the metallized portion's grain size at the bonding interface is less than $1\mu\text{m}$ due to the pressure during the bonding process; b. The grain size between the bond interface and the crack is approximately $10\mu\text{m}$, and the grain size above the crack is larger, which is the intrinsic grain characteristic of the unbonded wires; c. The crack propagates along with the interface between grain and original grain on the bonding interface. That is, the propagation path distance from the bonding interface is about one-grain length. Under the cyclic power stress, the crack propagates along the direction parallel to the bonding surface.

Under the working condition of periodic active heat generation of the device, the displacement information of the macroscopic model was used as the load boundary of the crystal model, and the crack growth process in the wedge-shaped structure of the bond wires obtained by using the micro-scale simulation model was shown in FIGURE 21.

Figure 21 (a) is the initial initiation stage of the crack, and the crack first initiation occurs at the leftmost bottom; (b) shows the initiation stage of the crack. The red color at the bottom left of the figure represents the formation of the crack and its expansion. (c) and (d) show the further propagation of the crack. It can also be seen in FIGURE 22(d) that crack initiation also occurs at the right bottom when the load is applied for a longer time.

According to the multi-scale IGBT power module bonding wires simulation model established in this paper, by curve fitting simulation results, the relationship between $L_{bond_crack_coh}$ and the loaded current cycle number N above the bonding wire interface can be expressed in segments as

$$L_{bond_crack_coh} = \begin{cases} 0 & N < 5783 \\ 2.209 \times 10^{-4} \times (N - 5783)^{1.342} \mu\text{m} & N \geq 5783 \end{cases} \quad (20)$$

Among them, in the 5783th cycle, it was found that the cohesive force unit damage reached 1. There was the crack

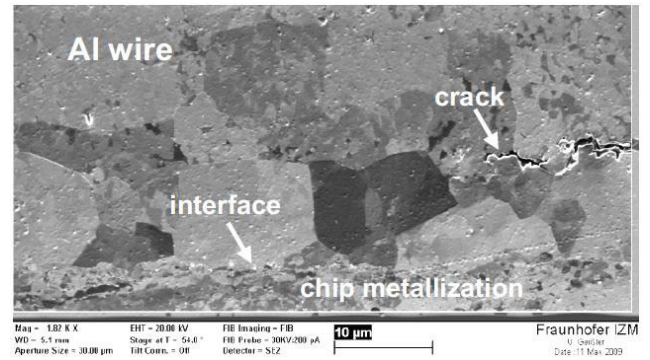


FIGURE 20. Micromorphology of crack propagation in bonding wires to IGBT power modules.

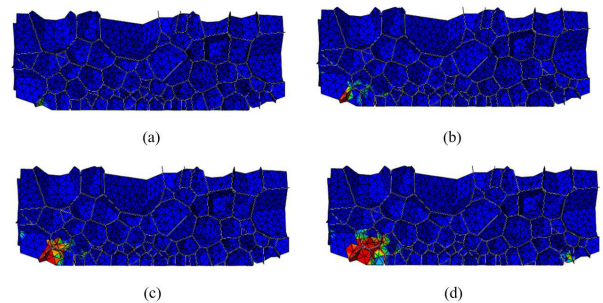


FIGURE 21. IGBT power module bond wires crack propagation process.

generation, before which the crack length was 0, and no crack was generated.

Because the cohesion model does not have thermal and electrical conductivity, there is no way to analyze the thermo-electric redistribution effect on a macro scale. $L_{bond_crack_coh}$ is the crack initiation and initial growth under the microscopic model. $L_{bond} = 2.00 \times 10^{-3}\text{m}$ is the total length of the bonding point. When the initial crack is less than 40% of the total length, the crack propagation law is described by the micro-level degradation behavior model. N is the number of cycles when the crack reaches the length threshold, which can be solved according to the micro-degradation behavior model. When the initial crack is 40% of the total length, The result is $N = 8.2 \times 10^4$.

The crack initiation and propagation behavior of the bonding wire are described from the microstructure, and the relationship between the crack length and the number of cycles is established.

V. EXPERIMENTAL VALIDATION

In this paper, a certain 1200V and 50A three-phase IGBT power integration module is selected as a specific object to carry out experiment application research. The device and related equipment of experimental verification have been introduced in Section III.B.

A. DESIGN OF POWER CYCLE SCHEME

Under the actual working conditions, the thermal cycle impact times of the device are far less than the power cycle

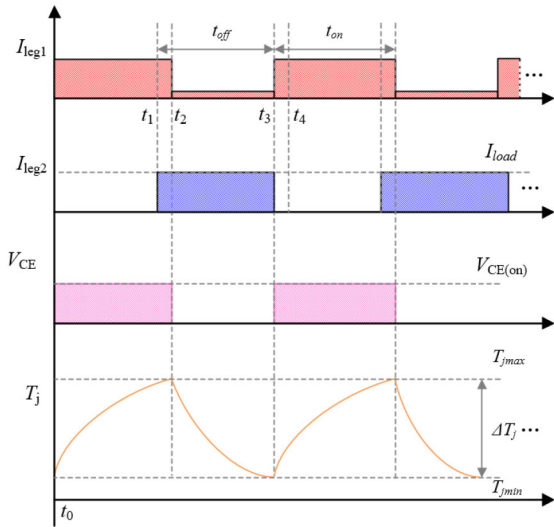


FIGURE 22. IGBT power cycle and junction temperature measurement profile.

impact caused by on-off, so the power cycle degradation test can better simulate the actual degradation process of the device [37]. The existing research results show that the cycle time of the fast power cycle test is less than 10 seconds and the junction temperature difference is large ΔT 100k is more likely to cause the bonding to lead to failure [38].

To simulate the actual ageing process of the IGBT power module, this paper adopts the power cycle test at equal intervals to age the IGBT power module to simulate the active heating and ageing process.

The tested device was fixed on the radiator, and the tested IGBT power module was aged through the load current I_{load} . The control of the circuit mainly relied on the upper two IGBT power modules as the main switch to realize dual current switching. The test current $I_{measure}$ and the voltage measurement module were used to obtain the conduction voltage drop $V_{CE(on)}$.

In the power cycle test, the IGBT chip generated periodic power dissipation in the state. When the junction temperature reached the target temperature, the load current was disconnected, and when the junction temperature dropped to the lower temperature limit, the load current was turned on. The cycle repeats, the junction temperature then exhibited periodic rise and fall. The cross-section of the repeated fluctuating current applied in the test is shown in FIGURE 22. The small current of the device is applied throughout the entire power cycle. Since the power dissipation generated by the small current is minimal, the heat loss caused by the IGBT turning off the device can be ignored.

During the test, the external circuit was used to monitor the chip voltage drop of an IGBT chip path under high current and low current. The voltage monitored under high current was recorded as the on-voltage drop $V_{CE(on)}$. The voltage drop at the moment when the device was turned off was converted to the junction temperature T_j through the small current temperature calibration relationship. Performing linear fitting on

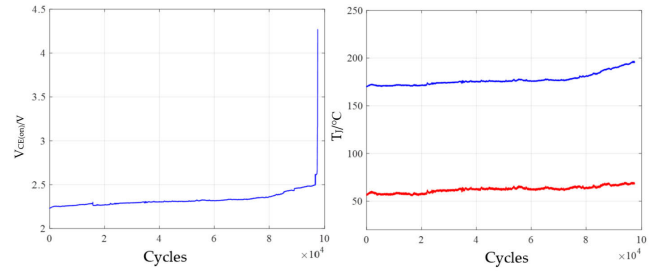


FIGURE 23. Parameter change curve monitored in the power cycle test.

TABLE 6. The IGBT power module power cycle test condition.

parameter	Collector current(I_c)	Turn on time(t_{on})	Turn off time(t_{off})	ambient temperature(t_a)
Test conditions	55A	2S	2S	293.15K

TABLE 7. Initial test data of power cycle test.

parameter	Turn-on voltage drop ($V_{CE(on)}$)	Maximum junction temperature ($T_{j,max}$)	Junction temperature difference ΔT_j	Minimum junction temperature ($T_{j,min}$)
Initial test data	2.382V	441.15K	112K	329.15K

the data obtained under different temperature and constant low current conditions, the relationship between the junction temperature T_j and the collector-emitter voltage drop V_{CE} is:

$$T_j = -330.6 \times V_{CE} + 326 \quad (21)$$

The test conditions set during the power cycle test are shown in Table 6. In the initial stage of the power cycle test, the initial data of the device obtained by the test are shown in Table 7.

B. TEST RESULTS AND ANALYSIS

As the bonding wires gradually fall off, the calculation will stop when the conduction voltage drop $V_{CE(on)}$ rises to the failure threshold, usually, 5%-20% can be selected. In this paper, 20% is selected as the failure criterion. If the port conduction voltage drop obtained by the simulation exceeds 20% of its initial value, it is judged as a device failure. Record the conduction voltage drop $V_{CE(on)}$ after each step, and obtain $V_{CE(on)}$ degradation law.

During the power cycle test, the conduction voltage $V_{CE(on)}$ and junction temperature T_j data of the IGBT power module are monitored, as shown in FIGURE 23Figure.

In the initial stage of the test, the device conduction voltage drop is relatively stable, the thermal resistance changes in a small range, and it is in a healthy state, about 6.4×10^4 cycles. The turn-on voltage drop of the device in the second stage enters a moderate degree of degradation. The cycle range is $6.4 \times 10^4 \sim 8.7 \times 10^4$ times; When the number of cycles is 6.4×10^4 times, the initial crack is 25% of the total length. When the number of cycles is 8.7×10^4 times, the initial crack is 40% of the total length and $V_{CE(on)}$ rises to the failure threshold. At the end of the module's life cycle, the bonding wires are damaged. Under the test conditions where the load



FIGURE 24. Bonding wires diagram after power cycle test.

current is 55 A and the temperature difference between the chip junction temperature is about 110°C, the main structural degradation and failure of the module is the degradation of the bonding wires.

In the early stage of the bonding wire degradation process, crack propagation has little effect on the voltage drop of the terminal. When the bond falls off, the voltage of the device changes significantly.

Analyze the degraded and failed IGBT, and use the BRUKER high-resolution three-dimensional tomography system SKYSCAN 2214 to obtain the appearance of the bonding wire, and the result shown in FIGURE 24 is obtained.

The bonding wire of the device has not found obvious shedding phenomenon, but the wire bonding strength after power cycling has decreased significantly, and the bonding force of the second bonding point of the two wires in the middle of the chip has been zero.

Through the power cycle aging test, the degradation of the bonding wire structure of the device is excited, and the degradation degree of the device is analyzed by using the monitoring degradation sensitive parameter data to further verify the correctness of the method.

VI. CONCLUSION

In this paper, a new multiscale model accounting for IGBT modules at the micro and macro-scales has been proposed to characterize the crack evolution in bonding wires. Firstly, the principle of the cohesive force model considering fatigue damage accumulation is analyzed, and the degradation simulation method of the critical structure of the power module is studied. Secondly, a macro-scale multi-physics coupling model was established to obtain the displacement information of the modular structure under cyclic loading. The Cohesive Zone Model is used to analyze the degradation behavior of the IGBT module's bond-wires based on the macroscopic node displacement information at the micro scale. The defect evolution model of the IGBT power module key package structure is established to analyze the damage evolution process of the critical package structure. The crack initiation and propagation length of the critical package structure of

the power module based on microstructural degradation were obtained by the simulation model. Finally, a case is given to verify the accuracy of the simulation model. It is worth noting that the proposed method provides accurate insights into the multi-scale bond wire degradation model and crack growth process.

REFERENCES

- [1] Y. Song and B. Wang, "Survey on reliability of power electronic systems," *IEEE Trans. Power Electron.*, vol. 28, no. 1, pp. 591–604, Jan. 2013.
- [2] T. J. Kilinski, J. R. Lesniak, and B. I. Sandor, "Modern approaches to fatigue life prediction of SMT solder joints," in *Solder Joint Reliability*. New York, NY, USA: Springer, 1991.
- [3] H. Lu, C. Bailey, and C. Yin, "Design for reliability of power electronics modules," *Microelectron. Rel.*, vol. 49, nos. 9–11, pp. 1250–1255, Sep. 2009.
- [4] K. C. Norris and A. H. Landzberg, "Reliability of controlled collapse interconnections," *IBM J. Res. Develop.*, vol. 13, no. 3, pp. 266–271, May 1969.
- [5] I. F. Kovacevic, U. Drogenik, and J. W. Kolar, "New physical model for lifetime estimation of power modules," in *Proc. Int. Power Electron. Conf.*, Jun. 2010, pp. 2106–2114.
- [6] Y. Celnikier, L. Benabou, L. Dupont, and G. Coquery, "Investigation of the heel crack mechanism in Al connections for power electronics modules," *Microelectron. Rel.*, vol. 51, pp. 965–974, May 2011.
- [7] L. Yang, P. A. Agyakwa, and C. M. Johnson, "Physics-of-failure lifetime prediction models for wire bond interconnects in power electronic modules," *IEEE Trans. Device Mater. Rel.*, vol. 13, no. 1, pp. 9–17, Mar. 2013.
- [8] W. Lai, M. Chen, L. Ran, S. Xu, L.-M. Pan, O. Alatisse, and P. Mawby, "Study on lifetime prediction considering fatigue accumulative effect for die-attach solder layer in an IGBT module," *IEEJ Trans. Electr. Electron. Eng.*, vol. 13, no. 4, pp. 613–621, Apr. 2018.
- [9] S. Abrate, J. F. Ferrero, and P. Navarro, "Cohesive zone models and impact damage predictions for composite structures," *Meccanica*, vol. 50, no. 10, pp. 2587–2620, Oct. 2015.
- [10] Z. Sun, L. Benabou, and P. R. Dahoo, "Prediction of thermo-mechanical fatigue for solder joints in power electronics modules under passive temperature cycling," *Eng. Fract. Mech.*, vol. 107, pp. 48–60, Jul. 2013.
- [11] L. Zhao, Y. Gong, and J. Zhang, "Research progress on lamination expansion behavior of fiber reinforced composite laminates," *J. Aviation*, vol. 40, no. 1, pp. 171–199, 2019.
- [12] F. Zhang and J. Zhao, "The application of cohesive elements in numerical simulations of the intergranular fracture in Voronoi cellular models," *Tool Autom. Manuf. Techn.*, vol. 55706, no. 11, pp. 26–29, 2013.
- [13] K. Zhang, B. Holmedal, O. S. Hopperstad, and S. Dumoulin, "Modelling the plastic anisotropy of aluminum alloy 3103 sheets by polycrystal plasticity," *Model. Simul. Mater. Sci. Eng.*, vol. 22, no. 7, Oct. 2014, Art. no. 075015.
- [14] F. Grytten, B. Holmedal, O. S. Hopperstad, and T. Børvik, "Evaluation of identification methods for YLD2004-18p," *Int. J. Plasticity*, vol. 24, no. 12, pp. 2248–2277, Dec. 2008.
- [15] B. Gao, F. Yang, M. Chen, L. Ran, I. Ullah, S. Xu, and P. Mawby, "A temperature gradient-based potential defects identification method for IGBT module," *IEEE Trans. Power Electron.*, vol. 32, no. 3, pp. 2227–2242, Mar. 2017.
- [16] A. S. Bahman, K. Ma, and F. Blaabjerg, "A lumped thermal model including thermal coupling and thermal boundary conditions for high-power IGBT modules," *IEEE Trans. Power Electron.*, vol. 33, no. 3, pp. 2518–2530, Mar. 2018.
- [17] C. Hager, "Lifetime estimation of aluminium wire bonds based on computational plasticity," ETH Zürich, Zürich, Switzerland, 2000, pp. 26–42, vol. 1, no. 3.
- [18] D. S. Dugdale, "Yielding of steel sheets containing slits," *J. Mech. Phys. Solids*, vol. 8, no. 2, pp. 100–104, 1960.
- [19] G. I. Barenblatt, "The mathematical theory of equilibrium cracks in brittle fracture," in *Advances in Applied Mechanics*, vol. 7. Amsterdam, The Netherlands: Elsevier, 1962, pp. 55–129.
- [20] G. I. Barenblatt, "The formation of equilibrium cracks during brittle fracture. General ideas and hypotheses. Axially-symmetric cracks," *J. Appl. Math. Mech.*, vol. 23, no. 3, pp. 622–636, Jan. 1959.

- [21] L. Zhao, Y. Gong, J. Zhang, Y. Chen, and B. Fei, "Simulation of delamination growth in multidirectional laminates under i and mixed mode I/II loadings using cohesive elements," *Compos. Struct.*, vol. 116, pp. 509–522, Sep. 2014.
- [22] L. Benabou, Z. Sun, and P. R. Dahoo, "A thermo-mechanical cohesive zone model for solder joint lifetime prediction," *Int. J. Fatigue*, vol. 49, pp. 18–30, Apr. 2013.
- [23] V.-N. Le, L. Benabou, Q.-B. Tao, and V. Etgens, "Modeling of intergranular thermal fatigue cracking of a lead-free solder joint in a power electronic module," *Int. J. Solids Struct.*, vols. 106–107, pp. 1–12, Feb. 2017.
- [24] B. A. E. van Hal, R. H. J. Peerlings, M. G. D. Geers, and O. van der Sluis, "Cohesive zone modeling for structural integrity analysis of IC interconnects," *Microelectron. Rel.*, vol. 47, no. 8, pp. 1251–1261, Aug. 2007.
- [25] S. Raghavan, I. Schmadlak, G. Leal, and S. K. Sitaraman, "Mixed-mode cohesive zone parameters for sub-micron scale stacked layers to predict microelectronic device reliability," *Eng. Fract. Mech.*, vol. 153, pp. 259–277, Mar. 2016.
- [26] B. Yang, S. Mall, and K. Ravi-Chandar, "A cohesive zone model for fatigue crack growth in quasibrittle materials," *Int. J. Solids Struct.*, vol. 38, nos. 22–23, pp. 3927–3944, May 2001.
- [27] K. L. Roe and T. Siegmund, "An irreversible cohesive zone model for interface fatigue crack growth simulation," *Eng. Fract. Mech.*, vol. 70, no. 2, pp. 209–232, Jan. 2003.
- [28] Q. Guo, "Study on fatigue fracture characteristics of wire bonding interface of power module," Zhejiang Univ. Technol., Hangzhou, China, 2017, pp. 14–49, vol. 1, no. 2.
- [29] C. Dresbach, M. Mittag, M. Petzold, E. Milke, and T. Müller, "Mechanical properties and microstructure of heavy aluminum bonding wires for power applications," in *Proc. Eur. Microelectron. Packag. Conf.*, Jun. 2009, pp. 1–8.
- [30] G. Khatibi, M. Lederer, B. Weiss, T. Licht, J. Bernardi, and H. Danninger, "Accelerated mechanical fatigue testing and lifetime of interconnects in microelectronics," *Procedia Eng.*, vol. 2, no. 1, pp. 511–519, Apr. 2010.
- [31] A. Grams, T. Prewitz, O. Wittler, J. Kripfgans, S. Schmitz, A. Middendorf, W. H. Müller, and K.-D. Lang, "Simulation of an aluminum thick wire bond fatigue crack by means of the cohesive zone method," in *Proc. 14th Int. Conf. Thermal, Mech. Multi-Phys. Simulation Exp. Microelectron. Microsyst. (EuroSimE)*, Apr. 2013, pp. 1–8.
- [32] T. Luther and C. Könke, "Polycrystal models for the analysis of intergranular crack growth in metallic materials," *Eng. Fract. Mech.*, vol. 76, no. 15, pp. 2332–2343, Oct. 2009.
- [33] K. B. Pedersen, D. Benning, P. K. Kristensen, V. N. Popok, and K. Pedersen, "Interface structure and strength of ultrasonically wedge bonded heavy aluminium wires in Si-based power modules," *J. Mater. Sci., Mater. Electron.*, vol. 25, no. 7, pp. 2863–2871, Jul. 2014.
- [34] R. Armstrong, I. Codd, R. M. Douthwaite, and N. J. Petch, "The plastic deformation of polycrystalline aggregates," *Phil. Mag., J. Theor. Exp. Appl. Phys.*, vol. 7, no. 73, pp. 45–58, Jan. 1962.
- [35] V. N. Popok, S. Buhrkal-Donau, B. Czerny, G. Khatibi, H. Luo, F. Iannuzzo, and K. B. Pedersen, "Comparative study of wire bond degradation under power and mechanical accelerated tests," *J. Mater. Sci., Mater. Electron.*, vol. 30, no. 18, pp. 17040–17045, Sep. 2019.
- [36] J. Goehre, M. Schneider-Ramelow, U. Geißler, and K. Lang, "Interface degradation of Al heavy wire bonds on power semiconductors during active power cycling measured by the shear test," in *Proc. 6th Int. Conf. Integr. Power Electron. Syst.*, Mar. 2010, pp. 1–6.
- [37] V. Smet, F. Forest, J. J. Huselstein, F. Richardeau, Z. Khatir, S. Lefebvre, and M. Berkani, "Ageing and failure modes of IGBT modules in high-temperature power cycling," *IEEE Trans. Ind. Electron.*, vol. 58, no. 10, pp. 4931–4941, Oct. 2011.
- [38] T. Herrmann, M. Feller, J. Lutz, R. Bayerer, and T. Licht, "Power cycling induced failure mechanisms in solder layers," in *Proc. Eur. Conf. Power Electron. Appl.*, 2007, pp. 1–7.



JUN LUO received the B.S. degree in microelectronics from Jilin University, in 2004, the M.S. degree in electronic science and technology from the University of Electronic Science and Technology of China, in 2009, and the Ph.D. degree in microelectronics and solid-state electronics from Xidian University, in 2018.

He is currently working with Sichuan Institute of Solid-State Circuits, China Electronics Technology Group Corporation. His research interests include microelectronics and solid state electronics, semiconductor integrated circuit, and failure analysis of semiconductor devices.



SHUKAI GUAN was born in Shandong, China, in 1996. He received the B.S. degree in safety science and engineering from the China University of Geosciences, Beijing, China, in 2019. He is currently pursuing the Ph.D. degree in systems engineering with Beihang University, Beijing. His research interests include reliability analysis for manufacturing process, simulation of solder joint fatigue, and reliability evaluation for electronic systems.



BO WAN (Member, IEEE) received the B.S. degree in mathematics and the M.S. and Ph.D. degrees in systems engineering from Beihang University, Beijing, in 2005, 2008, and 2017, respectively.

He is currently a Lecturer with the Institute of Reliability Engineering, Beihang University. His research interests include reliability simulation, reliability evaluation for electronics, and failure analysis.



MAOGONG JIANG was born in Heilongjiang, China, in 1992. He received the B.S. and Ph.D. degrees in electronic and information engineering from Beihang University, Beijing, China, in 2014 and 2020, respectively. He is currently working with the China Aerospace Components Engineering Center, Beijing. His current research interests include device modeling, failure analysis of semiconductor devices, power electronics reliability, and condition monitoring.



GUICUI FU (Member, IEEE) received the B.S. degree in mechanical manufacturing technology and design from Shenyang Aerospace University, Shenyang, China, in 1990, the M.S. degree in flight vehicle design from Northwestern Polytechnical University, Xi'an, China, in 1993, and the Ph.D. degree in flight vehicle design from Beihang University, Beijing, China, in 2005.

She is currently a Professor of systems engineering with Beihang University, where she is also the Deputy Director of the Research Center for Component Quality Engineering. Her research interests include electrical devices qualification assurance, engineering failure analysis, manufacturing process reliability, and physics of failure theories.

...